Artificial intelligence assessment of the jugular venous pulse from ultrasound high-resolution B-mode clips: A proof of concept

Paolo Zamboni, MD,[a,b,c] Anselmo Pagani, MSc,[b] Giulia Baldazzi, MD,[a,b] Saverio Farsoni, MSc, PhD,[d] Pietro Busi, MD,[e] Chiara Marchesin, MD,[e] Antonino Proto, MSc,[f] *and* Alessandro Bertagnon, MSc, PhD,[g] *Ferrara, Italy*

ABSTRACT

Objective: The jugular venous pulse (JVP) is a pivotal clinical parameter that currently can only be invasively measured through jugular catheterization and subsequent central venous pressure measurement. The ultrasound B-mode clip of the internal jugular vein cross-sectional area modifications allows to build a JVP curve that significantly correlates with the central venous pressure. However, this process is time-consuming and not suitable for clinical use. The aim of the present study is to verify whether artificial intelligence (AI) allows a rapid and reliable JVP waveform assessment as compared with a human operator.

Methods: High-resolution B-mode internal jugular vein clips (558 frames) of a cohort of six human subjects have been blindly analysed in post-processing by three different researchers and a neural network. Agreement was quantified using two complementary measures: Dice similarity coefficient (Dice) and the Hausdorff distance at the 95th percentile (HD95). Furthermore, a noninferiority test was performed comparing the model with the human raters. The null hypothesis (H0) was that the model performs worse than human raters by at least $\Delta = 0.055$ Dice, a difference that is considered clinically negligible.

Results: The average processing time per frame was 19.80 ± 5.08 seconds for human operators, compared with 0.03404 seconds ± 0.01806 seconds for the AI model running on a standard consumer-grade laptop. This represents a difference of nearly three orders of magnitude (a difference that could be quantitatively described as 580 times faster). Agreement between human raters was very high, with median Dice 0.959 (95% confidence interval, 0.958-0.960). Agreement between the model and each rater was slightly lower, with a median Dice of approximately 0.907 (95% confidence interval, 0.904-0.909). Human raters had median HD95 values of <5 pixels, reflecting very small boundary differences. The model-vs-rater comparisons showed somewhat higher HD95 values, with medians or approximately 8 to 10 pixels, but still within a clinically acceptable range given the resolution of the images. The Wilcoxon paired test rejected the null hypothesis H_0 ($P = .004169$), showing that the model is not inferior to human raters within this clinically acceptable margin.

Conclusions: Our study demonstrates an amazing time efficiency of the entire AI segmentation process, with a precision quite comparable with the human researchers' assessment. Our findings, in perspective, support the clinical introduction of ultrasound AI JVP waveform assessment in a variety of potentially interested medical specialties, including cardiology, critical care, neurosciences, and vascular surgery. (JVS-Vascular Insights 2026;4:100349.)

Keywords: Artificial intelligence; Jugular venous pulse; Internal jugular vein; Segmentation; Ultrasound; Neural network

The jugular venous pulse (JVP) is a reliable marker for pressure changes in the heart throughout the cardiac cycle.[1–5] The JVP is a pivotal physiological parameter for assessing cardiac filling, pump function of the heart, venous return, and cerebral drainage.[1] Currently, the JVP is qualitatively assessed in clinical practice, but its quantification can only be done by an invasive approach, through jugular catheterization and subsequent central venous pressure (CVP) measurement. However, it has been recently demonstrated that the JVP can be also extrapolated from ultrasound high resolution B-mode clips of the internal jugular veins (IJVs) synchronized with the electrocardiogram (ECG).[6,7]

The JVP waveform is composed of three ascents and three descents waves, which correspond with the

From the School of Vascular Surgery,[a] Department of Translational Medicine and for Romagna,[b] Vascular Diseases Center,[c] Department of Engineering,[d] School of Medicine, Department of Translational Medicine and for Romagna,[e] Department of Neuroscience and Rehabilitation,[f] and the Department of Environmental and Prevention Sciences,[g] University of Ferrara.

Additional material for this article may be found online at https://www.jvsvi.org.

Correspondence: Giulia Baldazzi, MD, School of Vascular Surgery, University of Ferrara, Via A. Moro 8, Ferrara 44124, Italy (e-mail: giulia01.baldazzi@edu.unife.it).

The editors and reviewers of this article have no relevant financial relationships to disclose per the Journal policy that requires reviewers to decline review of any manuscript for which they may have a conflict of interest.

2949-9127

http://dx.doi.org/10.1016/j.jvsvi.2025.100349

pressure variation of the cardiac phases: atrial contraction (wave *a*) synchronized with the P peak of the ECG, followed by atrial relaxation (wave *x*) and tricuspid valve closure (wave *c*). After the QRS complex of the ECG, the ventricular systole starts while passive atrial filling occurs followed by pressure drops. Subsequently, after the T peak of ECG corresponding with ventricular repolarization, the maximum atrial filling will be obtained (wave *v*) before the tricuspid valve opening. This latter causes a sudden pressure to decrease, coincident with ventricular filling (wave *y*), and then the JVP cycle will start again (Fig 1). The accuracy of the curve depends on the resolution of the ultrasound equipment. We need to perform a post analysis of approximately 40 different cross-sectional areas (CSAs) of the IJVs for each heartbeat to obtain and build a very reliable noninvasive trace of the JVP.[6,7]

In further experiments, it has been investigated whether the ultrasound JVP may provide a consistent estimation of CVP.[8] Therefore, by means of the lagging autocorrelation r-values as predictors, the mean CVP was calculated with reasonable accuracy by ultrasound JVP ($r^2 = 0.612$), with a mean absolute error of 1.455 cmH_2O.[8]

The main problem is the length of the postprocess analysis of the CSA changes from the B-mode clip. The investigators manually contour the IJV wall 200 times per every 5 heartbeats. The time required makes this method inapplicable in clinical practice. However, such a diagnostic methodology has the great advantage of being significantly correlated with the gold standard CVP, a parameter that can only be collected invasively via vein catheterization, a method not free from complications.

The main aim of the present study was to verify whether artificial intelligence (AI) allows a rapid and consistent post analysis of the sequence of the CSA modifications the IJV, to replace the long time required for a human to postprocess the contour and to allow this promising application of venous ultrasound examination to then be useful in clinical practice.

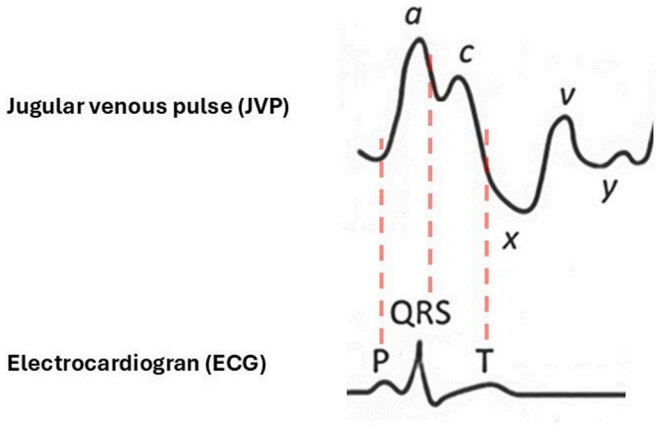

Fig 1. Jugular venous pulse (*JVP*) waveform peaks correlated with electrocardiogram (*ECG*) signal.

ARTICLE HIGHLIGHTS

- **Type of Research:** Comparative study between artificial intelligence (AI) and three human operators
- **Key Findings:** The average of segmentation time of a single frame of the internal jugular vein area, obtained from B-mode ultrasound clips, was 19.80 ± 5.08 seconds for human and 0.03404 ± 0.01806 seconds for AI with acceptable agreement (median Dice, 0.907; 95% confidence interval, 0.904-0.909) and significant noninferiority to human raters ($P = .004169$).
- **Take Home Message:** AI segmentation process, after training, is faster and can be comparable with human operators

METHODS

To enable a rigorous comparison between AI and human operators, the study was structured in sequential phases. In the first phase, we implemented and trained a neural network to reliably identify, delineate, and segment the anatomical structures (IJV and common carotid artery) within the recorded frames. The clinical data were managed locally without the use of cloud services and anonymized in compliance with privacy and cybersecurity requirements. In the subsequent phase, we compared the performance in imaging segmentation of the neural network and of three experienced human operators on completely unknown high-resolution B-mode IJV clips.

Network architecture and training strategy. We used a U-Net-based convolutional neural network for vessel segmentation, incorporating squeeze-and-excitation attention to improve the detection of vascular structures despite ultrasound noise.[9,10] The encoder backbone was a DenseNet-121 pretrained on RadImageNet, which offers a stronger and more clinically relevant initialization than conventional ImageNet.[11] RadImageNet is specifically designed around radiological image characteristics, such as medical texture patterns and intensity distributions, making its features better aligned with ultrasound imaging and therefore more effective for segmentation tasks trained on modestly sized datasets. A detailed dissertation about the network architecture and training strategies is available for the readers and can be found in the Supplementary Appendix (online only).

The network received three-channel ultrasound frames and produced three output classes (background, IJV, and carotid artery). Although the primary target of interest was the IJV, we deliberately adopted a multiclass design that also included the carotid artery. This choice

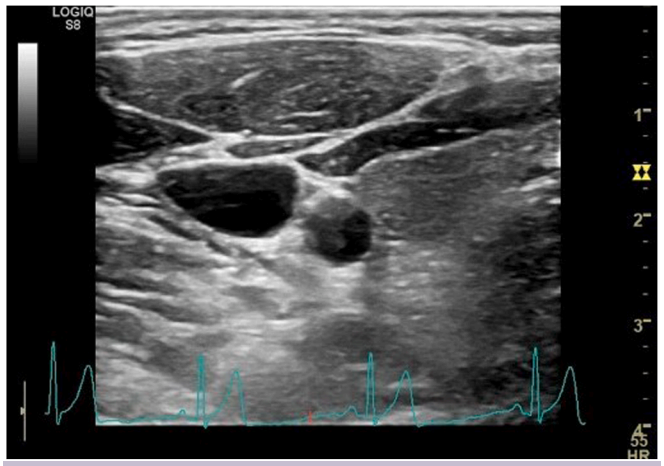

Fig 2. Echocardiographic clip frame used for artificial intelligence (AI) analysis, collected by a human sonographer, with the contemporary electrocardiogram (ECG) signal acquisition. The ECG allows to identify the ascents and descents of the jugular venous pulse (JVP) waveform inside a single beat.

was motivated by the anatomical proximity and frequent coappearance of the two vessels in ultrasound frames. By learning both structures simultaneously, the network could exploit their spatial relationships and relative positioning, leading to more stable and consistent segmentation of the jugular vein, even in challenging conditions such as overlapping shadows or partial vessel visibility.

To train the network, we adopted a hybrid loss function combining the Dice similarity coefficient[12-14] and the Hausdorff distance transform loss.[15-17] Dice loss was selected because it directly optimizes for overlap between predicted and reference masks, counteracting the strong class imbalance that characterizes vessel segmentation tasks, where the vessel lumen occupies a small fraction of the image. However, Dice loss alone may overlook local boundary errors, which can be clinically relevant when measuring vessel diameters. To address this limitation, the Hausdorff distance loss was included, because it emphasizes contour accuracy and penalizes deviations at the vessel boundaries. The combination of these losses thus balances volumetric accuracy with precise delineation of vessel walls.[18] The short clips were obtained after Ethical Committee approval (July 5, 2023) without considering demographics and comorbidities of the patients to avoid bias of selection. We used for all recording the same ultrasound machine (LOGIQ S8 with XDclear, GE HealthCare Technologies) and a linear probe (frequency range, 7-12 MHz) to bilaterally visualize and record the IJV and the common carotid artery in a transverse view at J2 level, far from any bone and/or muscular interference, with the subject in apnea.[19] We set the frame rate at 30 Hz, for precisely capturing CSA variations of the vein along the cardiac cycle; the latter was visualized through the ECG signal of the patients that was synchronized during image recording (Fig 2).

A total of 4528 frames were used for training and 1139 for validation. Images were resized to 256 $\times$ 256 pixels and normalized using RadImageNet statistics. The model was trained for $\leq$200 epochs with early stopping to reduce the risk of overfitting. Data augmentation was applied to improve generalization and robustness to acquisition variability. Elastic deformations were used to mimic probe-induced anatomical distortions, horizontal flips-simulated orientation changes, brightness and contrast variations reproduced differences in acquisition conditions, and Gaussian noise modelled ultrasound speckle. Validation data underwent only resizing and normalization to ensure comparability.

Training and validation loss curves (Fig 3) showed stable convergence without signs of overfitting, and qualitative inspection confirmed accurate vessel delineation, even in low-contrast or noisy ultrasound frames.

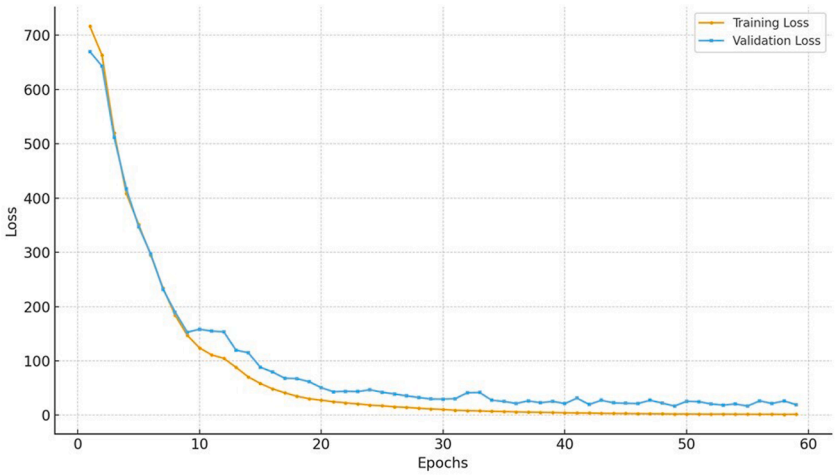

Fig 3. Training and validation loss over epochs.

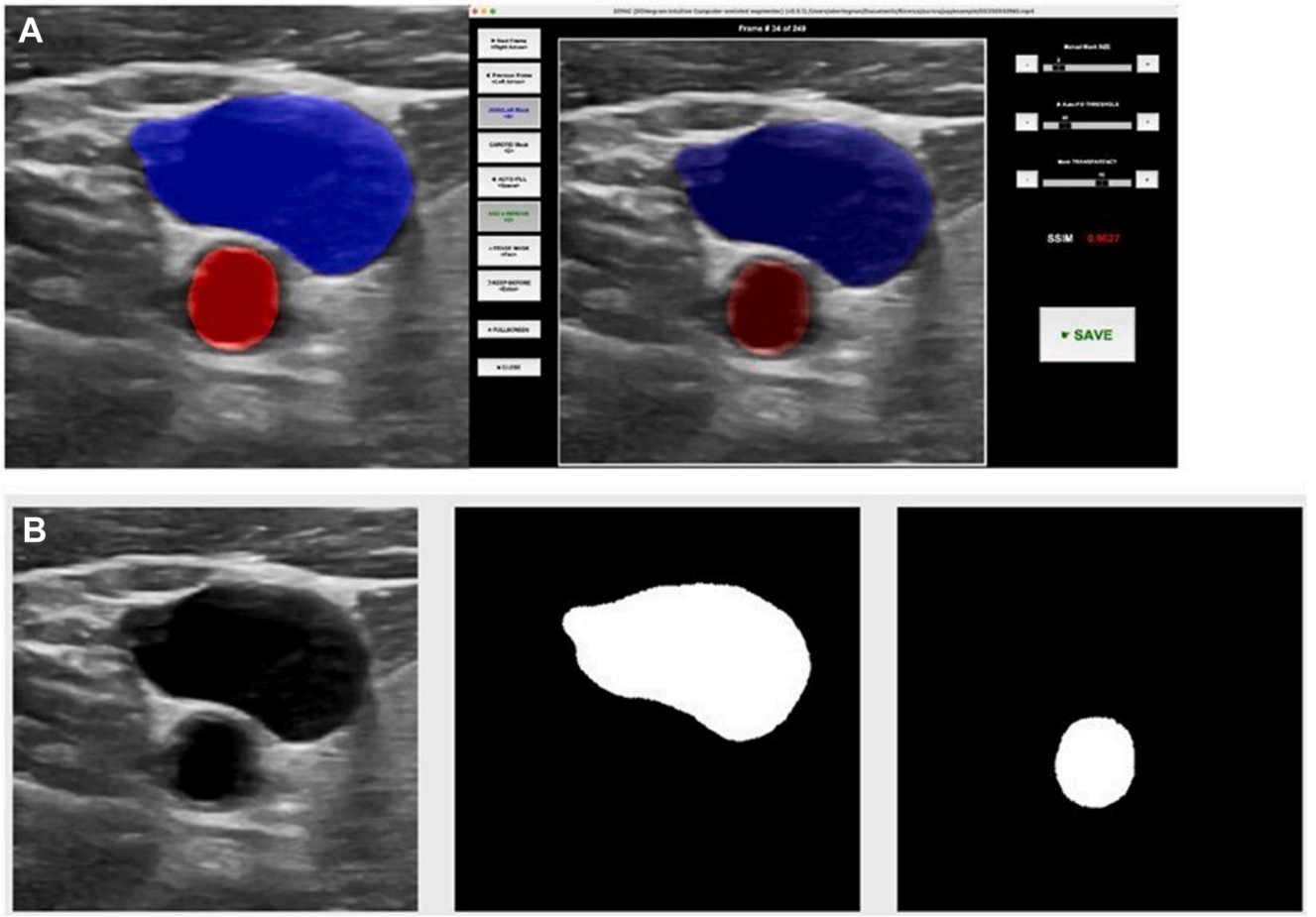

Fig 4. (A) Manual labelling by a human rater of the internal jugular vein (IJV) (*blue*) and common carotid artery cross-sectional areas (CSAs) (*red*). **(B)** Artificial intelligence (AI) system detecting IJV (*middle*) and common carotid artery (*right*) CSAs.

Comparison between the neural network and the human operators. To evaluate the reliability of the automatic segmentation, we compared three independent human raters (Fig 4, *A*) with the neural network (Fig 4, *B*) on segmentation of a total of unknown 558 frames, obtained from 6 healthy volunteers. These subjects have been selected among the researchers of the Department of Engineering to avoid any bias linked with cardiac rhythm, obesity, and neck vascular malformation. The B mode clips were insonated by P.Z., a vascular surgeon with 40 years of experience in the vascular laboratory; B.G., a vascular surgeon and PhD candidate in the field; and A.P., a PhD with a master's in vascular ultrasound and extensive research collaboration with NASA for pre and post flight IJV assessment of the astronauts. The manual contour of each of the IJV frames were performed by A.Pa., A.Pr., bioengineer and assistant professor in medical physics, and P.B., an MD as a part of his doctoral thesis in medicine. Human operators employed for the segmentation the software "SONIC" (implemented by one of the authors, an expert on AI [A.B.]) and contoured the area of the IJV (Fig 4, *A*, *blue*) and of the common carotid artery (Fig 4, *A*, *red*).

Agreement was quantified using two complementary measures. The Dice similarity coefficient (Dice) evaluates the overlap between two binary segmentations and ranges from 0 (no overlap) to 1 (perfect overlap). A Dice value of 0.90 means that 90% of the segmented pixels overlap, which is generally interpreted as excellent agreement in medical imaging. The Hausdorff distance at the 95th percentile (HD95) measures how far the boundaries of two segmentations are from each other, excluding the 5% worst outliers. It is expressed in pixels and therefore reflects boundary accuracy: lower values correspond with closer agreement of the segmented contours.

A majority-vote consensus mask was also computed to provide a robust reference. For each pixel, the label assigned by the three raters was considered, and the pixel was classified as vessel if at least two raters marked it as vessel. This technique reduces the impact of individual variability and represents the collective decision of the experts.

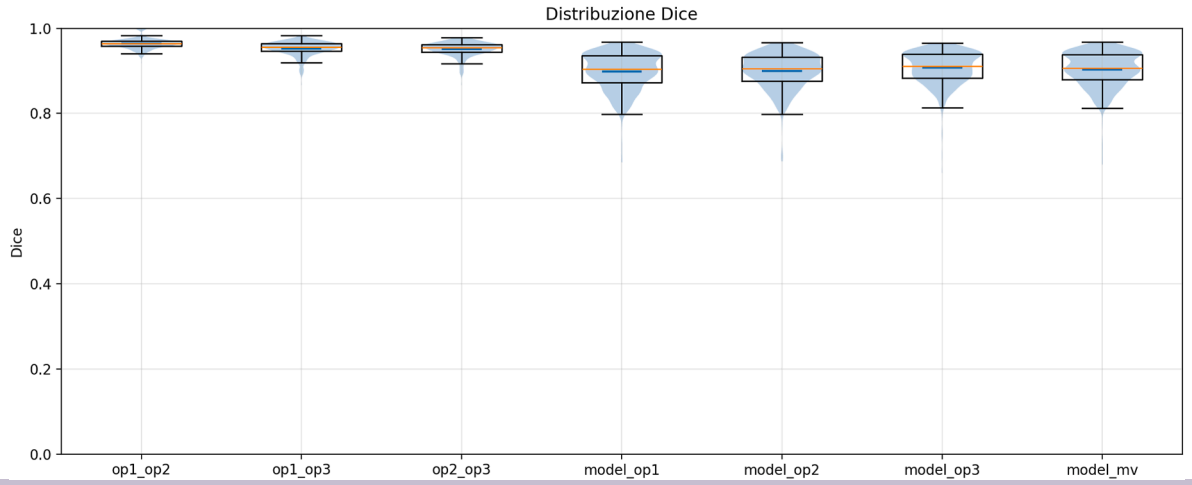

Fig 5. Distribution of Dice similarity coefficient between pairs of human raters and between the neural network and each rater. Higher values indicate better overlap.

RESULTS

The health subjects were composed by three males and three females with a mean age of 34.0 ± 3.3 years. Agreement between human raters was very high, with median Dice 0.959 (95% confidence interval, 0.958-0.960), as shown in Fig 5. Agreement between the model and each rater was slightly lower, with the median Dice around 0.907 (95% confidence interval, 0.904-0.909), but still within the range considered excellent for clinical segmentation tasks. Importantly, when comparing the model to the majority-vote consensus of the three raters, the Dice coefficient remained close to 0.91, highlighting that the neural network performance is comparable with human inter-rater agreement.

Human raters had median HD95 values of <5 pixels, reflecting very small boundary differences (Fig 6). The model-vs-rater comparisons showed somewhat higher HD95 values, with medians around 8 to 10 pixels, but still within a clinically acceptable range given the resolution of the images. This finding suggests that the network boundaries are very close to those of human raters, with deviations in the order of a few pixels, which does not influence the clinical significance.

Quantitative analysis confirmed these findings. The pooled mean Dice for model-vs-rater comparisons was 0.90 ± 0.04. Precision and recall values were 0.85 and 0.96, respectively, and the overall accuracy was 0.98. These values indicate that the model tends to slightly oversegment compared with human raters, but captures nearly all the target structure. At the level of anatomical areas, the intraclass correlation coefficient (2,1) was 0.94, which is interpreted as excellent agreement. Correlations between model and individual raters for area estimates were also high, with R^2 values ranging from 0.76 to 0.80.

We further evaluated the clinical significance of the differences using a noninferiority test. The null hypothesis was that the model is worse than the human raters by at least $\Delta = 0.055$ Dice. This margin corresponds with a 5.5% difference in segmentation overlap, which in practical terms represents only a small fraction of the vessel CSA. Given the image resolution (1 cm corresponds with 128 pixels, so 1 cm^2 corresponds with 16.384 pixels2), a $\Delta = 0.055$ Dice corresponds with an error of approximately 900 pixels2, or about 5 to 6 mm^2 of area. This error is negligible compared with the physiological variability of vessel dimensions. For context, the interoperator variability in our dataset already corresponds with differences of a similar or greater magnitude. The Wilcoxon paired test rejected the null hypothesis ($P = .004169$), showing that the model is not inferior to human raters within this clinically acceptable margin. This result supports the interpretation that the observed differences are negligible for clinical use.

On a consumer-grade computer (MacBook Pro 2023, Apple M2 Pro, 32 GB RAM), the model achieved an average inference time of 28.5 ms per frame (approximately 35 frames per second). The end-to-end processing time, including pre- and post-processing, was 0.03404 ± 0.01806 seconds per frame (approximately 29 frames per second). In contrast, a human rater requires on the order of 19.80 ± 5.08 seconds per frame, with segmentation quality likely to decrease over time owing to fatigue.

DISCUSSION

The main finding of the present study is that AI-based segmentation process demonstrated substantial time efficiency, while maintaining a level of precision comparable with that of the human raters, without performance degradation. Human operators required a

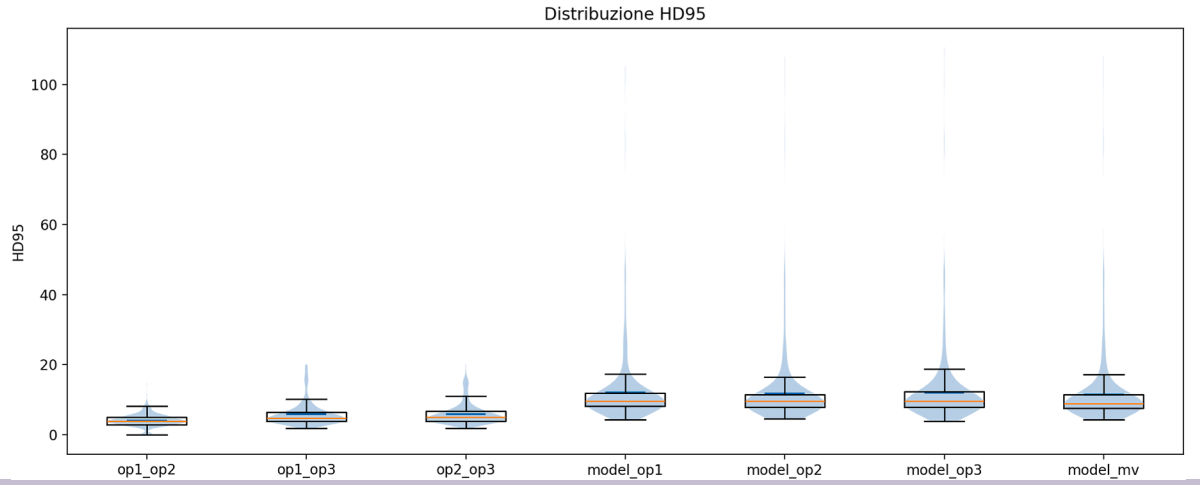

Fig 6. Distribution of 95th percentile Hausdorff distance (*HD95*) between pairs of human raters and between the neural network and each rater. Lower values indicate closer agreement of the segmentation boundaries.

mean of 19.80 ± 5.08 seconds to encircle a single frame of the IJV CSA from B-mode ultrasound clips; this means that a single JVP cycle requires a process of approximately 13 minutes. Of course, this cannot be proposed in the clinical settings. The speed of CSA segmentation, instead, is a key advantage of the neural network: AI completed the same task within only a few milliseconds (0.03404 ± 0.01806 seconds), making our methodology highly suitable for real-time clinical applications.

It has been demonstrated that autocorrelation values of IJV-CSA measured by human sonographers correspond reliably with the CVP.[8] In clinical practice, there are three main relevant ranges of CVP: ≤0 to 3 cmH_20, corresponding with hypovolemia; 4 to 8 cmH_20, a normal range; and ≥9, hypervolemia. Thus, the differences assessed between the human operators and AI, in the present study, are completely negligible: we know that the mean IJV-CSA in a cohort of healthy subject at J1 is 48 mm^2, as compared with 5 mm^2 of error between a human rater and AI.[20]

This result let us conclude that the real-time AI CSA assessment of the JVP might permit in the future to extrapolate a reliable noninvasive CVP value in clinical practice. Interestingly, our AI ultrasound methodology may have a variety of potential clinical applications: in critical care, in the emergency clinical setting to evaluate major bleedings rapidly and efficiently, in patient assessment after major surgeries, in cardiology especially to assess chronic heart failure,[2,3] in neurosciences,[21-23] and in vascular surgery,[24,25] as well to evaluate the cerebral venous outflow.

Moreover, the AI process can be used independently from any ultrasound equipment on the market, as long as high-resolution imaging (about 35-40 frames per heartbeat) is available. The heartbeat corresponds with the time variable of the *x* axis of the JVP waveform, normalized to the individual heart frequency.

The main limitation of the present study was that we analyzed exclusively healthy subjects. This was done to avoid further bias linked with diseases such as atrial fibrillation, tricuspid valve regurgitation, although we are planning further studies that will include such patients.

CONCLUSIONS

This study offers a new perspective on the use of AI in clinical practice for venous diseases, supporting health care personnel in a slow, laborious procedure that is prone to error. The robustness of the dataset used in the training phase plays the same role as its heterogeneity in the reliability expressed by this AI tool. Despite this pronounced difference in processing time, concordance between AI and human assessments remained high, with the AI approach demonstrating clear noninferiority to human performance. These findings collectively support the prospect of noninvasive JVP assessment across a range of medical specialties interested in such an important clinical parameter.

AUTHOR CONTRIBUTIONS

Conception and design: PZ, APa, AB
Analysis and interpretation: PZ, APa, GB, SF, AB
Data collection: PZ, APa, GB, PB, CM, APr
Writing the article: PZ, APa, GB, AB
Critical revision of the article: PZ, APa, GB, SF, PB, CM, APr, AB
Final approval of the article: PZ, APa, GB, SF, PB, CM, APr, AB
Statistical analysis: AB
Obtained funding: Not applicable

Overall responsibility: PZ

PZ and APa contributed equally to this article and share co-first authorship.

FUNDING

None.

DISCLOSURES

None.

REFERENCES

1. Mari S, Pagani A, Valentini G, et al. Monitoring the cerebral venous drainage in space missions: the Drain Brain experiments of the Italian Space Agency. *Veins and Lym*. 2023;12:27–33. http://dx.doi.org/10.4081/vl.2023.11716
2. Constant J. Using internal jugular pulsations as a manometer for right atrial pressure measurements. *Cardiology*. 2000;93:26–30. http://dx.doi.org/10.1159/000006998
3. Applefeld MM. The jugular venous pressure and pulse contour. In: Walker HK, Hall WD, Hurst JW, eds. *Clinical Methods: The History, Physical, and Laboratory Examinations*. 3rd ed. Butterworths; 1990 Chapter 19.
4. Irwin RS, Rippe JM, Celinski S, Snafu M. Central venous catheters. In: *Irwin and Rippe's Intensive Care Medicine*. 6th ed. Lippincott Williams & Wilkins; 2008:19–37.
5. Mackay IFS. An experimental analysis of the jugular pulse in man. *J Physiol*. 1947;106:113–118. http://dx.doi.org/10.1113/jphysiol.1947.sp004197
6. Sisini F, Tessari M, Gadda G, et al. An ultrasonographic technique to assess the jugular venous pulse: a proof of concept. *Ultrasound Med Biol*. 2015;41:1334–1341. http://dx.doi.org/10.1016/j.ultrasmedbio.2014.12.666
7. Zamboni P, Sisini F, Menegatti E, et al. Ultrasound monitoring of jugular venous pulse during space missions: proof of concept. *Ultrasound Med Biol*. 2018;44:726–733. http://dx.doi.org/10.1016/j.ultrasmedbio.2017.11.001
8. Zamboni P, Malagoni AM, Menegatti E, et al. Central venous pressure estimation from ultrasound assessment of the jugular venous pulse. *PLoS One*. 2020;15:e0240057. http://dx.doi.org/10.1371/journal.pone.0240057
9. Roy AG, Navab N, Wachinger C. Concurrent spatial and channel 'Squeeze & Excitation' in fully convolutional networks. In: *In Medical Image Computing and Computer Assisted Intervention – MICCAI 2018: 21st International Conference, Granada, Spain, September 16-20, Proceedings, Part I*. Springer-Verlag, Berlin, Heidelberg; 2018:421–429. http://dx.doi.org/10.1007/978-3-030-00928-1_48
10. Ronneberger O, Fischer P, Brox T. U-Net: Convolutional networks for biomedical image segmentation. In: Navab N, Hornegger J, Wells W, Frangi A, eds. *Medical Image Computing and Computer-Assisted Intervention – MICCAI 2015. Miccai*. Lecture Notes in Computer Science; 9351.
11. Mei X, Liu Z, Robson PM, et al. RadImageNet: an open radiologic deep learning research dataset for effective transfer learning. *Radiol Artif Intell*. 2022;4:e210315. http://dx.doi.org/10.1148/ryai.210315
12. Dice LR. Measures of the amount of ecologic association between species. *Ecology*. 1945;26:297–302. http://dx.doi.org/10.2307/1932409
13. Sørensen T. A method of establishing groups of equal amplitude in plant sociology based on similarity of species content and its application to analyses of the vegetation on Danish commons. *Biologiske Skrifter/Kongelige Danske Videnskabernes Selskab*. 1948;5:1–34.
14. Milletari F, Navab N, Ahmadi SA. V-Net: fully convolutional neural networks for volumetric medical image segmentation. In: *Proceedings of 2016 Fourth International Conference on 3D Vision (3DV)*. 2016:565–571. http://dx.doi.org/10.1109/3DV.2016.79
15. Hausdorff F. *Grundzüge der Mengenlehre*. Leipzig Veit; 1914.
16. Dubuisson MP, Jain AK. A modified Hausdorff distance for object matching. In: *Proceedings of 12th International Conference on Pattern Recognition, Vol. 1 – Conference A: Computer Vision & Image Processing*. IEEE; 1994:566–568. http://dx.doi.org/10.1109/ICPR.1994.576361
17. Karimi D, Salcudean SE. Reducing the Hausdorff distance in medical image segmentation with convolutional neural networks. *IEEE Trans Med Imaging*. 2020;39:499–513. http://dx.doi.org/10.1109/TMI.2019.2926400
18. Kingma DP, Ba J. Adam: a method for stochastic optimization. In: *International Conference on Learning Representations (ICLR)*. 2015. Submitted on 22 Dec 2014 (v1), last revised 30 Jan 2017 (this version, v9) arXiv:1412.6980v9.
19. Zamboni P, Menegatti E, Pomidori L, et al. Does thoracic pump influence the cerebral venous return? *J Appl Physiol (1985)*. 2012;112:904–910. http://dx.doi.org/10.1152/japplphysiol.00712.2011
20. Zamboni P, Sisini F, Menegatti E, et al. An ultrasound model to calculate the brain blood outflow through collateral vessels: a pilot study. *BMC Neurol*. 2013;13:81. http://dx.doi.org/10.1186/1471-2377-13-81
21. Zhou D, Ding JY, Ya JY, et al. Understanding jugular venous outflow disturbance. *CNS Neurosci Ther*. 2018;24:473–482. http://dx.doi.org/10.1111/cns.12859
22. Zhou D, Meng R, Zhang X, et al. Intracranial hypertension induced by internal jugular vein stenosis can be resolved by stenting. *Eur J Neurol*. 2018;25:365-e13. http://dx.doi.org/10.1111/ene.13512
23. Zamboni P, Scerrati A, Menegatti E, et al. The eagle jugular syndrome. *BMC Neurol*. 2019;19:333. http://dx.doi.org/10.1186/s12883-019-1572-3
24. D'Oria M, Zlatanovic P, Anthony A, et al. International union of angiology consensus document on vascular compression syndromes. *Int Angiol*. 2023;42:282–309. http://dx.doi.org/10.23736/S0392-9590.23.05100-3
25. Zamboni P, Galeotti R, Salvi F, et al, Brave Dreams Research Group. Effects of venous angioplasty on cerebral lesions in multiple sclerosis: expanded analysis of the brave dreams double-blind, sham-controlled randomized trial. *J Endovasc Ther*. 2020;27:1526602819890110. http://dx.doi.org/10.1177/1526602819890110

Submitted Oct 16, 2025; accepted Dec 19, 2025.

Additional material for this article may be found online at https://www.jvsvi.org.